PCCP

PAPER

View Article Online
View Journal | View Issue

Cite this: *Phys. Chem. Chem. Phys.*, 2025, **27**, 24578

Tetrel-substituted pyramidanes as electron donors in noncovalent bonds

Mariusz Michalczyk, *[a] Steve Scheiner [b] and Wiktor Zierkiewicz [a]

Received 3rd September 2025,
Accepted 20th October 2025

DOI: 10.1039/d5cp03390j

rsc.li/pccp

The apex C atom of square pyramidane C(C_4H_4) is replaced by heavier tetrel T atoms Si, Ge, Sn, and Pb. The molecular electrostatic potential surrounding the substituted T-pyramidane features minima at both the apex and the square base. Quantum chemical calculations are conducted to examine the ability of these two sites to act as electron donors in H-bonds, halogen bonds, or osme bonds to group 8 metals Fe, Ru, and Os. Osme bonds are strongest, with some approaching 40 kcal mol^{-1}, with a heavy covalent contribution, followed by halogen and then by hydrogen bonding. The latter are fairly weak, with interaction energies between 0.6 and 3.3 kcal mol^{-1}. The apex T site is favored over the square base for osme bonds, but the base is preferred for H-bonds. There is a more delicate balance for halogen bonds, with Si preferred over the pyramid base, but the latter favored for Sn. The primary electron donor site at the apex is a pseudo-lone pair on T, while the π-electron system serves this function when the electrophile attacks the base of the pyramid.

Introduction

The pyramid shape has a very long history, beginning in antiquity, as a structure of special architectural and artistic significance. In the microscale world of chemistry, molecules of pyramidal shape have been the objects of extensive conjecture and research. The family of such molecules, containing only C and H, are commonly referred to as [*n*]pyramidanes, where *n* refers to the number of C atoms in the base.[1,2] The more formal name of [4]pyramidane, sometimes called simply pyramidane, would be tetracyclo-[2.1.0.0.^{1,3}0^{2,5}]pentane.[3] Its square planar cyclo-C_4R_4 base (where R denotes H or some other substituent) is connected *via* four C–C bonds to an apex tetracoordinated tetrel atom (usually carbon) as part of an inverted tetrahedral configuration.[4] The stability of the pyramidane scaffold is rooted in a large activation barrier of around 25 kcal mol^{-1}, which inhibits transformation to its ring-open carbene isomer.[1,5–8]

Interest in the pyramidal T(C_4R_4) structure, where T = Si, Ge, Sn, Pb, has become the subject of experimental research.[9–11] The following compounds have been synthetized: Si[C_4($SiMe_3$)$_4$][9] Ge[C_4($SiMe_3$)$_4$],[11] Sn[C_4($SiMe_3$)$_4$],[11] and T[T'_4(SiR_3)$_4$],[10] where T = Ge, Sn, Pb, T′ = C, Si, Ge, and R = Me, Me^{t}Bu$_2$. Along with this work, there have been a number of theoretical predictions[2,4,7,12–15] of their properties. Imagawa *et al.* synthesized several silapyramidanes, where Fe(CO)$_4$ interacted directly with an apical Si atom.[11] Borapyramidanes were synthesized by the Erker[16] group in 2022. Pendas *et al.* carried out theoretical studies on the electronic structure[2] of T[C_4($SiMe_3$)$_4$] pyramidanes, in which the apical T center was a tetrel atom, varying from C to Pb. Their analysis suggested that the interactions between apical and basal atoms changed from covalent to electrostatically driven as the tetrel atom size increased, with the exception of T = Si. Previous computational studies extended beyond isolated pyramidanes. For example, Veljkovic *et al.*[14] scrutinized the interactions between pyramidanes and water molecules. The molecular electrostatic potential (MEP) in the vicinity of the apex C atom was found to be negative (ranging from −49 to −8 kcal mol^{-1}) for a set of pyramidanes, depending on the substituents on the base C atoms. Such pyramidanes could thus behave as nucleophiles, interacting directly with H atoms of water. The study found strong O–H···C hydrogen bonds characterized by interaction energies reaching as high as −7.4 kcal mol^{-1}.[14] Decomposition of the interaction energy indicated the primary electrostatic character of these contacts.

A very recent computational work considered pyramidane in the context of other highly strained C atoms, and comparison was drawn with a set of propellanes.[15] The carbon atom at the apex served as an electron donor to a variety of different noncovalent bonds, including hydrogen, halogen, chalcogen, pnicogen and tetrel bonds, by taking advantage of the σ-holes[17,18] on the various electrophiles with which they were paired. Of the systems considered, the Sn···C tetrel bonds were strongest, up to 56 kcal mol^{-1}, bordering on a covalent bond.

[a] *Faculty of Chemistry, Wrocław University of Science and Technology, Wybrzeże Wyspiańskiego 27, 50-370 Wrocław, Poland. E-mail: mariusz.michalczyk@pwr.edu.pl*
[b] *Department of Chemistry and Biochemistry, Utah State University Logan, Utah 84322-0300, USA*

To be sure, the concentration of electron density at carbon atoms has been observed in several contexts. What is particularly notable is the ability of the strained C of propellanes and pyramidanes to serve as an electron donor despite the absence of a formal lone pair. This participation is aided by the presence of what might be thought of as a pseudo-lone pair orbital on this center.[10,15] It would thus appear that the electrostatic potential and electronic structure of the highly strained C of pyramidanes place it in the pantheon of electron sources for σ-hole bonds, joining the already established club of lone pairs and π- and σ-bonds.

The present work involves high-level calculations to better understand the origin of the curious interactions between pyramidanes and selected Lewis acids. In order to broaden the dataset which has largely concentrated on the C atom at the apex of the pyramid in the past, this C was replaced in turn by each of the larger tetrel T atoms (Si, Ge, Sn and Pb), which thus covers a wide range of atomic size and electronegativity, and response to bond strain. The type of bonding was also broadened by considering a set of nine different Lewis acids covering hydrogen, halogen, and osme bonding to group 8 metals Fe, Ru, and Os, one of the newly established types of noncovalent bonds.[19–22] The choice of the latter was motivated by the observation of a pyramidane crystalline solid with an $Fe(CO)_4$ group, which is stabilized by an Fe···Si osme bond.[11] To further broaden the types of interactions that pyramidanes are capable of forming, the calculations presented here suggest the possibility that an approaching electrophile can interact not with the apex, but rather with the base of the pyramid. The comparison of the bonding to these two very different sites on these pyramids provides additional insights into the bonding capabilities of tetrel atoms, and also concerning intermolecular interactions in a more general sense.

Methods

Full geometry optimizations of isolated monomers and dyads were performed at the M06-2X/def2-tzvpp[23–26] level of theory using the Gaussian 16 (Rev. C.01) package.[27] Harmonic frequency analyses verified that the optimized geometries are true minima. The counterpoise approach of Boys and Bernardi[28] was used to correct the basis set superposition error (BSSE). MultiWFN software[29,30] was used (a) to find the extrema of the MEP on the 0.001 a.u. electron isodensity surface, (b) to find the extrema of the average local ionization energy (ALIE) on the vdW surface, and (c) for ELF (electron localization function) analysis.[31,32] Graphical post-processing of wave function analyses was performed using VMD software.[33] QTAIM topological analysis of the electron density[34,35] was performed using the AIMAll program.[36] Decomposition of the interaction energy into its specific components was achieved using the ALMO-EDA scheme[37,38] within Q-Chem 6 software. NBO analysis[39] was employed to identify and quantify specific interorbital interactions and to obtain natural atomic charges. Additionally, atomic polar tensor (APT) charges were calculated.

Results

Monomers

Four pyramidane molecules with the general formula $T(C_4H_4)$, with T = Si, Ge, Sn or Pb, were fully optimized, and several selected features are listed in Table 1. The C–C bond distances at the base of each pyramid are all equal to one another, confirming the structure as a square pyramid. There is little variation in this bond length from one molecule to the next. The bond length to the T atom at the pyramid apex increases with the size of T, from 2.027 Å for Si up to 2.432 Å for Pb. The parameter h is defined as the height of the pyramid, from the center of the square base to the T at its apex. This height varies between 1.748 and 2.204 Å. These bond lengths are rather close to those computed earlier by Vidal *et al.*[2] for similar molecules containing $SiMe_3$ substituents on the four basal C centers.

The overall MEP values surrounding the pyramidanes are shown in Fig. 1 for the Si and Pb variants. Each contains a minimum directly above the T atom, but this minimum is not necessarily negative in sign. As listed in the fourth column of Table 1, $V_{s,min}$ on the 0.001 a.u. isodensity surface varies from a negative −9.4 kcal mol^{-1} for Si up to +18.3 kcal mol^{-1} for the more electropositive Pb. It is worth noting that there is another minimum at the base of each pyramid, which is more negative than that near T, as is clear from the next column of Table 1. As another perspective on this point, the ALIE (average local ionization energy) was computed as well. The results in Table 1 indicate that this quantity is smaller at the site of the apical tetrel atom than at the pyramid base. From this point of view, the former would be preferred over the latter as a site for electrophilic attack.

As another measure of the charge distribution, the last column of Table 1 displays the atomic polar tensor (APT) charges assigned to T. This charge is positive for all T, but becomes more so as the atom grows in size, consistent with the same trend in $V_{s,min}$(T). A similar pattern of more positive MEP for heavier T was reported earlier[2] for the $SiMe_3$ tetrasubstituted pyramidanes. For purposes of comparison, the MEP minimum near the apical C in $C(C_4H_4)$ was computed earlier[15] to be much more negative at −42.3 kcal mol^{-1}, consistent with carbon's

Table 1 Selected parameters for isolated pyramidanes (distances in Å, MEP minima in kcal mol^{-1}, ALIE minima in eV, and APT charges q in e)

Monomer	R(C–C)	R(C–T)	h	$V_{s,min}$(T)	$V_{s,min}$(base)	$I_{s,min}$(T)	$I_{s,min}$(base)	q(T)
$Si(C_4H_4)$	1.451	2.027	1.748	−9.4	−14.1	8.88	10.50	0.252
$Ge(C_4H_4)$	1.453	2.135	1.872	−4.7	−13.4	8.93	10.44	0.315
$Sn(C_4H_4)$	1.455	2.335	2.097	+3.2	−17.4	8.24	9.95	0.507
$Pb(C_4H_4)$	1.454	2.432	2.204	+18.3	−21.5	7.80	9.57	0.565

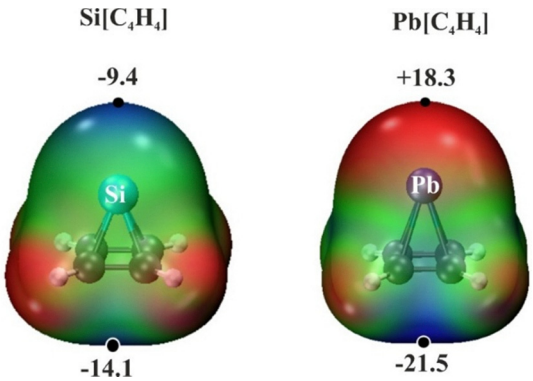

Fig. 1 MEPs of the Si and Pb variants of pyramidane molecules. Black dots indicate the location of MEP minima ($V_{s,min}$), with values in kcal mol^{-1}. The color scale is arranged from blue (−12.6 kcal mol^{-1}) to red (+12.6 kcal mol^{-1}).

higher electronegativity. This highly negative potential on the apical C persists as substituents are added to the basal C atoms.[14]

Another perspective on the electron density distribution of each pyramidane entity is derived from ELF analysis. The ELF basins are presented in Fig. 2 for an isovalue of 0.85 a.u. These basins can be divided into monosynaptic, V(T) (a T lone pair), and disynaptic, V(C,C) or V(C,H), as labelled in Fig. 2.

Of particular interest are the lone pair V(T) basins that progressively weaken in the Si < Ge < Sn order, vanishing entirely for Pb at this particular isovalue. Average population numbers in V(T) basins are 2.74e (Si), 2.86e (Ge), 2.68e (Sn) and 2.76e (Pb), nearly the same for all tetrel atoms despite the different sizes of these basins. NBO localization of the wavefunction of each monomer leads to the appearance of an orbital that closely resembles a lone pair on each tetrel atom, as is clear from Fig. S1. This orbital is primarily of s character, roughly 90%. Consistent with the near equality of the ELF populations, the NBO lone pairs are similar in appearance for all T. While ELF designates these areas as encompassing high electron localization, NBO formalism refers to the localized orbital here as a lone pair. In either scenario, these electrons are available for bonding with an electrophile.

Three different types of Lewis acids were tested as partners for these pyramidanes. The HX series, with X = F, Cl, Br, were examined as proton donors in H-bonds to the apical T atom. Another type of interaction examined was halogen bonds *via* the FX series, where it is the σ-hole on the X center that might interact with T. A third category allows the pyramidane T to interact with the central M atom of M(CO)$_4$ for the group 8 metals Fe, Ru, and Os in what might be classified as an osme bond. The values of $V_{s,max}$ on these various electrophiles are provided in Table S1. As expected, the value on the H of HX becomes less positive with larger X, while the opposite is true for the X center of FX. The MEP on the central M atom of M(CO)$_4$ is rather uniform for all three M, between 16.3 and 18.4 kcal mol^{-1}.

Apical dyads

Each of the nine electrophiles was paired with one of the four pyramidanes, allowing the bridging atom of the Lewis acid to

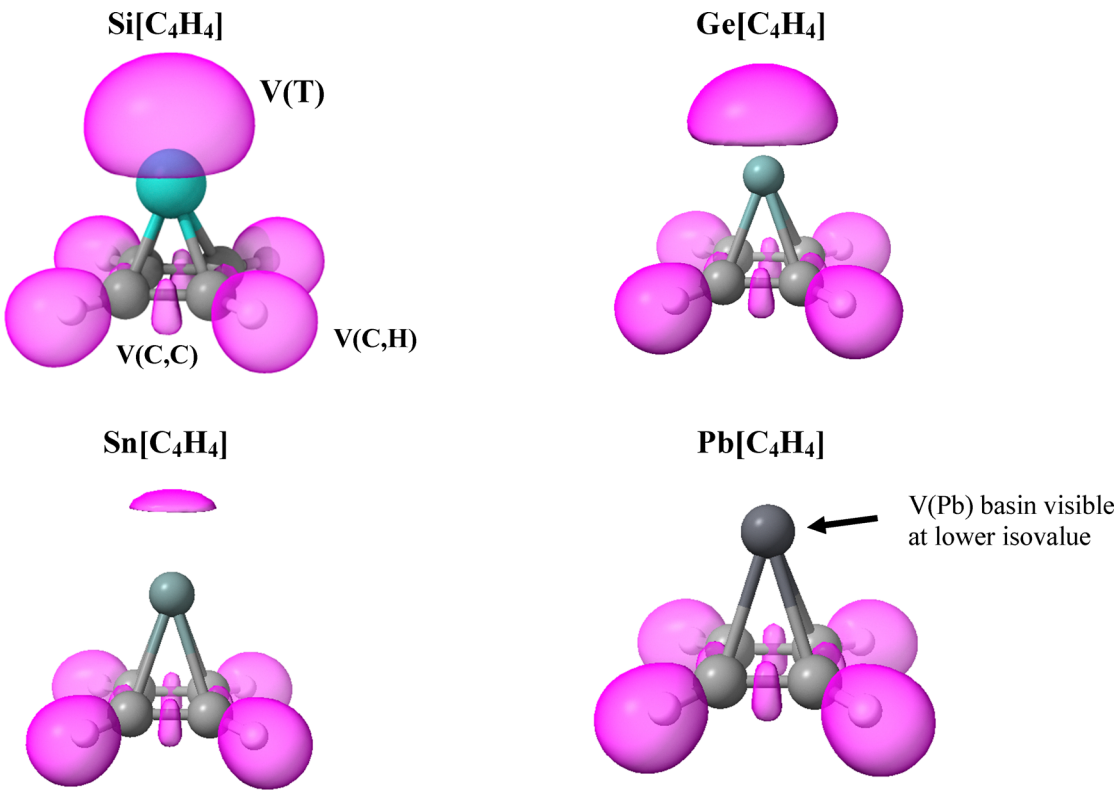

Fig. 2 ELF diagrams of pyramidanes with ELF basins indicated by pink globular shapes at an isovalue of 0.85 a.u.

approach the apical T atom. Probably due to the highly positive MEP at the Pb center, the Pb-pyramidanes were unable to form stable complexes with any of these Lewis acids (although stable interactions were observed with the negatively charged base of the Pb-pyramid; see below). The structures adopted by the three remaining pyramidanes with these various Lewis acids are illustrated in Fig. 3, which defines the key geometrical parameters. These quantities are collated in Table 2, where several patterns can be observed.

Both the HBs and XBs are very close to linear with θ and α values close to 180°. The one exception occurs for the FI··Sn XB, where α is only 140°. The Fe and Ru osme bonds are also linear with α values close to 180° with the exception of Sn. The complexes involving the osme bonds are based on a trigonal pyramidal shape around the metal center, with the pyramidane occupying an equatorial site. θ_1 refers to the angle made with one of the two axial C atoms, so it is close to 90° (89°–101°), whereas those involving the two equatorial C atoms are designated as θ_2, which is about 113°. Not unexpectedly, the intermolecular distances R grow with the size of the T atom in the order of Si < Ge < Sn. The same is generally true for the XB complexes and the size of X, with the exception of Sn, where this distance contracts from Cl to I. There is little sensitivity of the osme bonds to the identity of the M atom.

The M062X interaction energies are collected in Table 3, along with the same quantity calculated at the higher CCSD(T) level.

The latter reproduces the trends of the former, although there are some quantitative differences. CCSD(T) halogen bond energies are a bit smaller than those of M062X but follow the same trend. The same is true for the osme bonds, except that here the CCSD(T) values are systematically slightly larger in magnitude. At either level of theory, the osme bonds are rather strong, in the range between 18 and 40 kcal mol^{-1}. Os engages in the strongest of these, with Ru and Fe being comparable to one another. With respect to the pyramidanes, Si is the most potent electron donor. XBs are substantially weaker and HBs are weaker still, 3 kcal mol^{-1} or less. The XB pattern follows along with σ-hole depth on the electrophile: I > Br > Cl, and with $V_{s,min}$ on T: Si > Ge > Sn. As a parenthetical comment, it may be noted that Sn engages in all three types of bonds, despite its positive $V_{s,min}$.

AIM analysis of the electron density within the complexes reveals a bond path between the apical T and the atom of the Lewis acid with which it interacts directly (H, X, or M), as illustrated in the molecular diagrams in Fig. S1. The three most important parameters of this bond path are associated with the

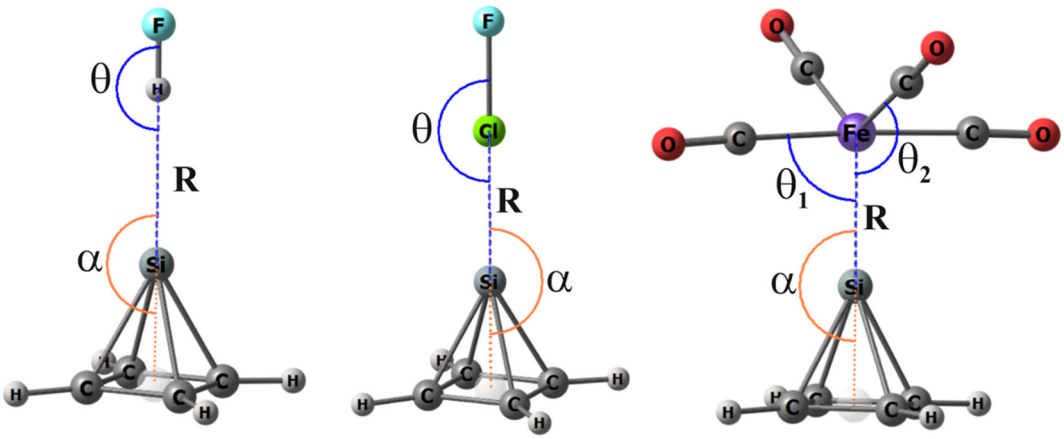

Fig. 3 Geometries of selected dimers, defining intermolecular parameters.

Table 2 Geometric parameters of complexes (interatomic distance R (Å) and angles θ and α (degrees) are shown in Fig. 2)

	Si(C_4H_4)			Ge(C_4H_4)			Sn(C_4H_4)		
	R	θ	α	R	θ	α	R	θ	α
HF	2.524	179.6	179.0	2.599	179.7	178.9	2.770	180.0	179.0
HCl	2.719	179.2	178.9	2.797	180.0	178.3	2.984	176.7	178.2
HBr	2.742	177.3	177.5	2.833	175.9	177.8	3.020	172.5	172.6
FCl	2.390	179.9	179.9	3.054	180.0	179.9	3.212	179.9	179.8
FBr	2.488	180.0	180.0	2.830	179.8	179.9	3.152	179.7	179.9
FI	2.686	179.9	179.9	2.905	179.1	173.0	3.042	179.0	139.5
$Fe(CO)_4$	2.202	88.6/116.7[a]	179.9	2.396	89.1/118.3[a]	176.8	2.574	89.2/117.5[a]	150.2
$Ru(CO)_4$	2.287	92.2/111.3[a]	179.9	2.490	93.8/112.2[a]	179.1	2.692	89.6/113.0[a]	133.4
$Os(CO)_4$	2.294	100.8/101.7[a]	179.9	2.448	93.8/111.3[a]	176.7	2.614	91.5/113.7[a]	144.7

[a] In osme bonded dimers, there are two variants of angle θ: θ_1/θ_2; see Fig. 3.

Table 3 Interaction energies of dyads (kcal mol^{-1})

	$Si(C_4H_4)$		$Ge(C_4H_4)$		$Sn(C_4H_4)$	
	M062X	CCSD(T)	M062X	CCSD(T)	M062X	CCSD(T)
HF	−3.33	−2.93	−2.37	−1.86	−1.39	−0.50
HCl	−1.93	−1.97	−1.34	−1.34	−0.68	−0.53
HBr	−1.73	−1.86	−1.18	−1.31	−0.61	−0.61
FCl	−10.13	−5.83	−3.36	−1.67	−2.72	−0.69
FBr	−13.91	−10.03	−5.98	−3.95	−4.50	−2.18
FI	−14.28	−11.59	−8.29	−6.15	−8.32	−5.44
$Fe(CO)_4$	−30.16	−39.84	−20.85	−28.30	−20.10	−26.12
$Ru(CO)_4$	−29.41	−34.62	−18.21	−23.63	−17.60	−22.29
$Os(CO)_4$	−38.04	−39.66	−25.02	−28.00	−27.08	−29.49

bond critical point: density ρ, potential energy density V, and total energy density H, all of which pertain to bond strength and type, and are compiled in Table 4.

Similar to the interaction energies, ρ is smallest for the HBs (0.008–0.015 a.u.), larger for the XBs (0.016–0.066 a.u.) and highest for the osme bonds (0.050–0.096 a.u.). The higher end of this spectrum approaches the 0.1 a.u. arbitrary border into covalency.[40] These patterns in ρ also bear some resemblance to the energetic ordering from Si to Ge and Sn. In fact, the correlation coefficient R^2 for a linear fit between these two quantities is 0.91. Similar patterns are observed for V, but of course with a different range of values. The correlation with E_{int} is even better for V with R^2 = 0.96. A negative value of H is commonly taken as a sign that the interaction contains a significant degree of covalency. With the exception of the HBs in the upper segment of Table 4, H is mostly negative, particularly so for the osme bonds.

A decomposition of the interaction energy into several physically meaningful components provides further perspective on the nature of the bonding. The results of ALMO-EDA decomposition of the interaction energies are displayed in Table 5.

The entries refer to the percent contribution of each of the four attractive elements, electrostatic (ES), polarization (POL), charge transfer (CT) and dispersion (DISP), to the total of all four. Focusing first on the HB complexes, those involving Si and Ge show roughly 50% contribution from ES that is typical of HBs in general. But ES is way down, less than 20%, for the Sn complexes, where all three of the other attractive elements have increased to make up the difference. The patterns are internally consistent within the osme bonds. ES accounts for roughly half, DISP is quite small on the order of 10%, and POL and CT make up the remainder in roughly equal amounts, although the latter tends to be a bit larger than the former. The XB data are rather interesting. ES tends to be largest for Ge as compared to Si or Sn. CT is quite substantial as well, comparable to ES and exceeding it in some cases. DISP is generally small; however, it does increase a bit for the Sn XB dyads. Polarization energy makes up the smallest percentage in most cases.

Table 5 Percentage contributions of ALMO-EDA decomposition terms of interaction energies for complexes (ES = electrostatic term, POL = polarization, CT = charge transfer, DISP = dispersion; percentage contributions are defined as the fraction of the sum of attractive elements

	$Si(C_4H_4)$				$Ge(C_4H_4)$				$Sn(C_4H_4)$			
	ES	POL	CT	DISP	ES	POL	CT	DISP	ES	POL	CT	DISP
HF	53	14	19	15	51	16	17	15	16	28	29	27
HCl	53	9	21	17	52	10	20	18	19	17	31	34
HBr	52	8	23	17	52	9	21	19	20	14	33	33
FCl	24	12	55	9	44	6	32	18	32	7	35	25
FBr	25	19	48	8	38	10	40	13	35	10	35	20
FI	43	17	29	11	42	12	32	14	39	12	34	15
$Fe(CO)_4$	44	18	30	8	51	16	24	9	58	13	19	11
$Ru(CO)_4$	58	12	24	6	60	9	24	7	57	10	23	9
$Os(CO)_4$	48	26	22	4	50	20	25	5	49	21	24	5

NBO localization of the MOs participating in these interactions provides a framework by which to consider the fundamental aspects of the bonding. Fig. 4 depicts the orbitals directly involved in the intermolecular bonding of $Sn(CH)_4$ as an example pyramidane. The Sn pseudo-lone pair is obvious for the HB and XB in Fig. 4(a) and (b), which donates a certain amount of charge to the σ^* antibonding orbitals in HF and ClF as prototypical HB and XB, as indicated by the curved red arrow. The osme bonding with $Ru(CO)_4$ is strong enough that NBO analyzes the density as containing a single entity, with the Ru–Sn bond shown in Fig. 4(c).

Another window into the nature of the bonding arises in connection with monitoring the way in which the electron

Table 4 AIM parameters (a.u.) within complexes at the bond critical point involving the apical T

	$Si(C_4H_4)$			$Ge(C_4H_4)$			$Sn(C_4H_4)$		
	ρ	V	H	ρ	V	H	ρ	V	H
HF	0.015	−0.008	−0.001	0.013	−0.006	0.000	0.011	−0.005	0.000
HCl	0.011	−0.005	0.000	0.010	−0.004	0.001	0.008	−0.003	0.001
HBr	0.011	−0.005	0.000	0.009	−0.004	0.001	0.008	−0.003	0.001
FCl	0.066	−0.047	−0.022	0.018	−0.010	0.001	0.016	−0.008	0.001
FBr	0.064	−0.045	−0.020	0.034	−0.021	−0.004	0.022	−0.012	−0.001
FI	0.053	−0.037	−0.014	0.036	−0.023	−0.006	0.034	−0.020	−0.005
$Fe(CO)_4$	0.081	−0.086	−0.039	0.058	−0.063	−0.019	0.050	−0.050	−0.013
$Ru(CO)_4$	0.089	−0.093	−0.050	0.067	−0.067	−0.024	0.055	−0.049	−0.015
$Os(CO)_4$	0.096	−0.104	−0.060	0.080	−0.082	−0.034	0.070	−0.068	−0.024

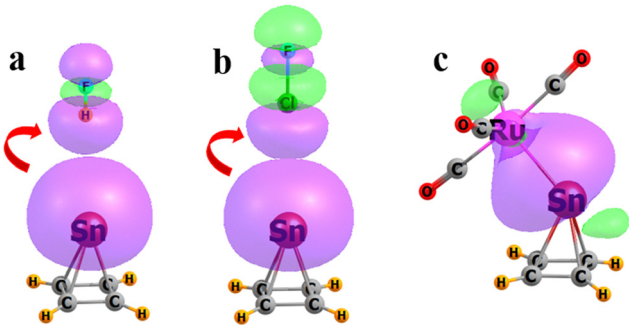

Fig. 4 Natural bond orbitals primarily responsible for the intermolecular bonding of $Sn(CH)_4$ with (a) HF, (b) ClF, and (c) $Ru(CO)_4$. Red arrows indicate the direction of electron flow.

density shifts when the two monomers approach so as to form the dyad. These maps were generated by subtracting the density of the two isolated monomers from that of the entire complex, and are displayed in Fig. 5 for several of these systems.

The green and red colors, respectively, signify areas of density accumulation and depletion resulting from the interaction. In each case, there is an extensive green region between the two subunits where the buildup of density helps to cement the two units together. A good deal of this extra density is extracted from the apical T atom, as indicated by the prominent red region encircling it. The polarizations occurring within the Lewis acid units are evident from the pattern of green and red lobes within each.

As in most complexation processes, the two monomers each undergo certain structural changes to accommodate their partner. The first column of Table 6 shows that there is a small stretch of the bonds between the four basal C atoms.

This stretch is minimal for the HBs but increases to as much as 0.016 Å for the osme-bonded dimers. Concomitant with the expansion of the base is a flattening of the pyramid as the four C–T bonds to the apical T contract by as much as 0.04 Å. The exceptions include the Sn-osme bonds to Ru and Os, where there is a small elongation. If one were to consider bond length changes as a barometer of bond strength, the three types of noncovalent bonds slightly weaken the C–C bonds within the square base, while strengthening the C–T bonds to the apex of the pyramid by a larger amount. The geometric changes caused by complexation raise the energy of each monomer relative to its fully optimized structure. This sum of deformation energies of the two subunits is collected in Table S2, where it can be seen to be fairly small in most cases, with the exception of the osme-bonded dimers, where E_{def} can exceed 8 kcal mol^{-1}. When E_{def} is subtracted from the interaction energy, one has the binding

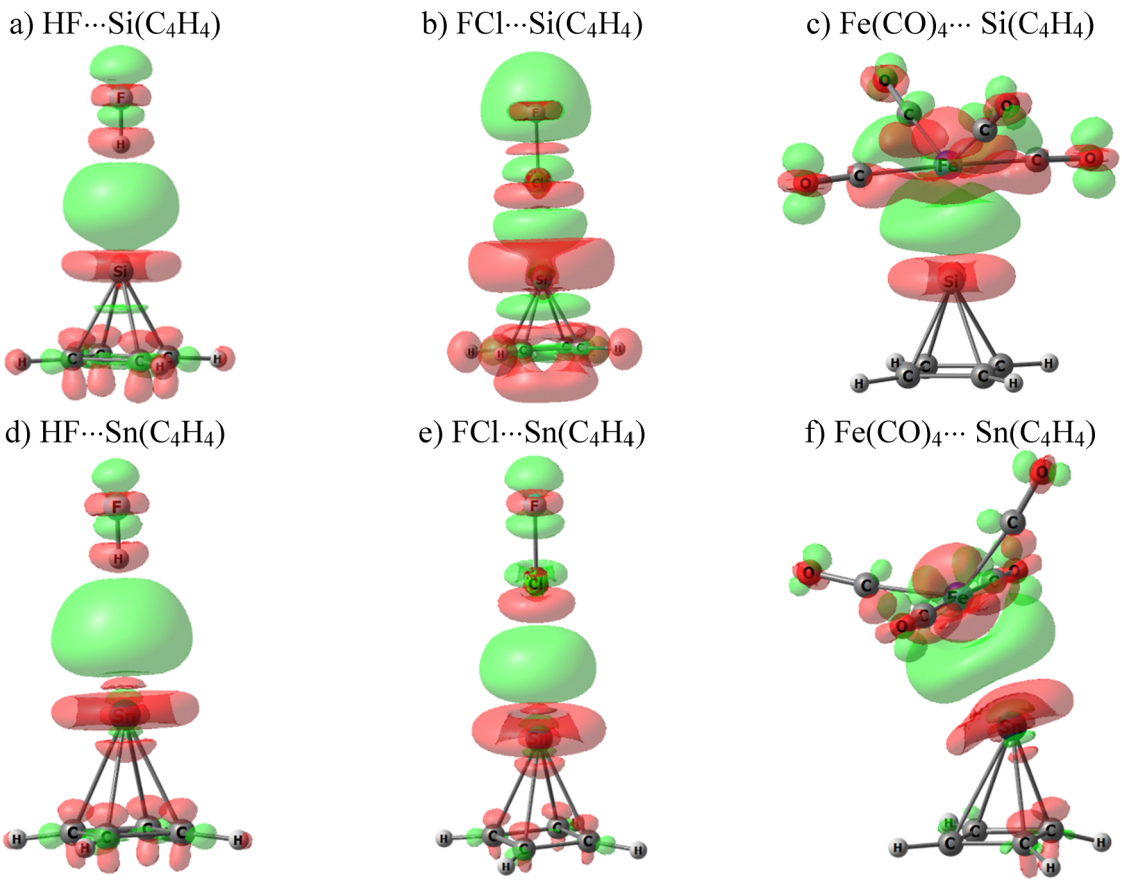

Fig. 5 Electron density shift occurring within labeled dyads. Green and red colors indicate regions of gain and loss of electron density, respectively. The contour shown is ±0.0005 for (a), (b), (d), and (e) and ±0.002 a.u. for (c) and (f).

Table 6 Changes in the internal bond lengths and charge on T of pyramidane due to complexation, along with the total charge transferred (CT) from pyramidane to the electrophile (bond lengths in Å and charges in *e*)

	$Si(C_4H_4)$				$Ge(C_4H_4)$				$Sn(C_4H_4)$			
	Δr(C–C)	Δr(C–T)	Δq_T	CT	Δr(C–C)	Δr(C–T)	Δq_T	CT	Δr(C–C)	Δr(C–T)	Δq_T	CT
HF	+0.002	−0.015	−0.040	0.02	+0.002	−0.017	−0.044	0.01	+0.001	−0.016	−0.036	0.01
HCl	+0.001	−0.010	−0.018	0.02	+0.001	−0.010	−0.027	0.01	+0.001	−0.012	−0.019	0.01
HBr	+0.001	−0.009	−0.008	0.03	+0.001	−0.010	−0.021	0.02	+0.002	−0.012	−0.013	0.01
FCl	+0.006	−0.037	0.256	0.34	+0.001	−0.015	0.006	0.05	+0.002	−0.015	0.021	0.05
FBr	+0.007	−0.042	0.233	0.32	+0.004	−0.028	0.075	0.14	+0.003	−0.025	0.051	0.09
FI	+0.007	−0.041	0.158	0.25	+0.009	−0.043	0.062	0.15	+0.011[a]	−0.012[a]	0.102	0.20
$Fe(CO)_4$	+0.006	−0.039	0.649	0.66	+0.011	−0.044	0.473	0.51	+0.006[a]	−0.006[a]	0.529	0.55
$Ru(CO)_4$	+0.004	−0.036	0.634	0.65	+0.005	−0.035	0.447	0.49	+0.015[a]	+0.005[a]	0.459	0.52
$Os(CO)_4$	+0.007	−0.042	0.561	0.58	+0.002	−0.043	0.458	0.50	+0.016[a]	+0.013[a]	0.563	0.59

[a] Average value.

energy E_b equal to the reaction energy from optimized monomers to the optimized dyad. These quantities are listed in Table S3, where it is clear that they follow the same pattern as that of E_{int}, even if a bit smaller in magnitude.

Also listed in Table 6 as Δq_T are the changes in the natural charge on the apical T atom when involved in the bond to each of the Lewis acids. This atom becomes more negative in the various HBs, particularly for the strong proton donor HF. This density increase is typical of HB proton acceptor atoms and is likely attributable in large measure to internal polarization within the pyramidane that makes the T a more attractive target for the positively charged bridging proton. The tetrel atom increases its positive charge for the XBs, especially noticeable for FI with its deep σ-hole on I. This density loss is consistent with the red regions surrounding T in Fig. 5. The increase in positive charge is very substantial for the osme-bonded complexes, roughly 0.5*e*. This large change is consistent with the high degree of covalent character of these bonds. The last column in each section of Table 6 lists the total amount of charge displaced from the pyramidane to the electrophilic molecule. This CT is small for the HBs, a bit larger for the stronger XBs, and very large, on the order of 0.5–0.7*e*, for the OsBs. These large intermolecular charge transfers are consistent with the density loss from T signaled by its substantially more positive charge, as well as the red areas in Fig. 5 within the pyramidanes. These effects are similar for the XBs, if a bit muted.

Interactions with the pyramidane base

As shown in Table 1, the MEP near the base of these pyramidanes is more negative than that in the neighborhood of their apex, sometimes by quite a bit. It is therefore no surprise that an electrophile might find the base an inviting site at which to engage in a noncovalent bond. Indeed, all four of the pyramidanes, including that containing Pb, formed such a complex with all nine of the electrophiles considered. A selection of several of these complexes with $Si(C_4H_4)$ are illustrated in Fig. 6, and the interaction energies of the entire set are collected in Table 7; their deformation energies and the ensuing binding energies are reported in Tables S4 and S5, respectively. As in the apical structures, the osme bonds are strongest, followed by halogen, and then by hydrogen bonds. These quantities conform fairly closely to the basal $V_{s,min}$, following the pattern Pb > Sn > Ge ≈ Si.

The AIM molecular diagrams are displayed on the right side of Fig. S2. They show bond paths leading to various elements of the base, either a C atom or a C–C bond midpoint. The AIM parameters for these intermolecular bond paths are collected in

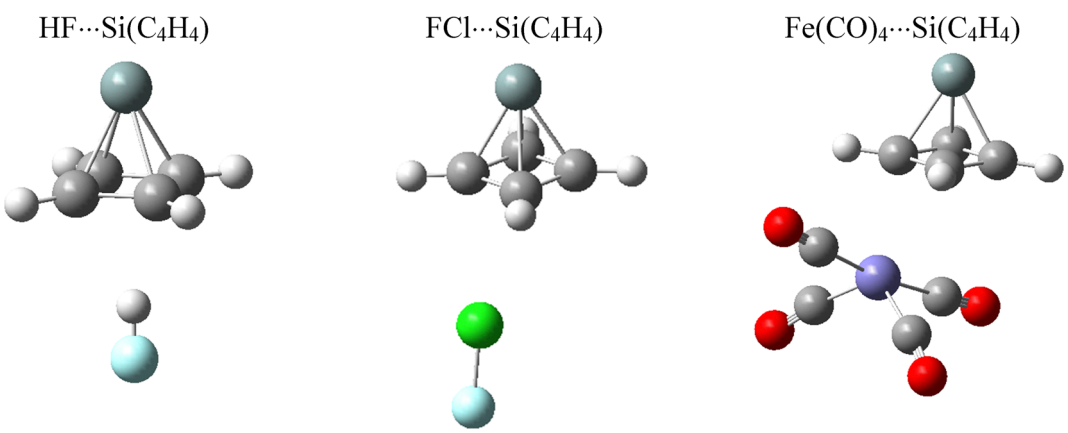

Fig. 6 Geometries of selected basal dimers.

Table 7 Interaction energies of the basal dimers (kcal mol^{-1})

	$Si(C_4H_4)$		$Ge(C_4H_4)$		$Sn(C_4H_4)$		$Pb(C_4H_4)$	
	M062X	CCSD(T)	M062X	CCSD(T)	M062X	CCSD(T)	M062X	CCSD(T)
HF	−5.18	−3.73	−5.02	−3.64	−5.70	−3.91	−6.24	−4.22
HCl	−3.98	−3.20	−3.88	−3.15	−4.47	−3.31	−4.91	−4.78
HBr	−3.77	−3.18	−3.70	−3.10	−4.31	−3.35	−4.72	−3.57
FCl	−4.50	−2.58	−4.53	−2.62	−5.51	−3.04	−6.29	−3.45
FBr	−6.16	−4.18	−6.23	−4.28	−7.98	−5.30	−10.55	−6.88
FI	−7.89	−5.61	−7.98	−5.77	−10.36	−7.42	−13.03	−9.24
$Fe(CO)_4$	−12.64	−13.64	−12.66	−13.82	−15.48	−16.90	−17.03	−18.48
$Ru(CO)_4$	−8.65	−8.56	−8.77	−8.83	−10.44	−10.42	−11.67	−11.57
$Os(CO)_4$	−9.72	−9.60	−9.93	−10.03	−14.17	−14.58	−17.31	−17.75

Table S6. The bond critical point densities remain clearly in the noncovalent range, all less than 0.05 a.u. The total energy density *H* hovers around zero, confirming only a minor degree of covalency.

NBO analysis of the density of each complex allows for a better understanding of the orbitals involved in the bonding. This protocol reapportions the total density into a series of orbitals that are highly localized. The C_4 structure of the base of the pyramid is represented by a group of four σ(C–C) bonding orbitals, one for each pair of adjacent C atoms. This array is supplemented by one C–C π bonding orbital. The HB and XB complexes in Fig. 7(a) and (b) show the recipient orbital in each case to be the pertinent σ* orbital of the Lewis acid. The primary donor in the HCl case of Fig. 7(a) can be described as a Ge–C bonding orbital, comprising a C π-orbital, that overlaps nicely with the HCl σ*. The chief donor in the XB case is the π bonding orbital between a pair of C atoms in the base of the pyramid. The same CC π orbital is the primary donor to the Fe atom in Fig. 7(c). The orbital within $Fe(CO)_4$, which accepts charge, is labeled by NBO as a vacant Fe lone pair orbital, primarily of p-character, with its main lobe pointing toward the pyramid base. This sort of osme bonding also contains a contribution from back-bonding. Specifically, some charge is transferred from the Fe d-orbital in Fig. 7(d) to a CC π* antibonding orbital within the pyramidane. The latter accounts for a second-order perturbation energy of 7.8 kcal mol^{-1}, as compared to 20.8 kcal mol^{-1} for the main transfer in Fig. 7(c).

As for the apical complexes, the effect of H-bonding on the basal C–C bond lengths is very little, as is evident from Table S7. On the other hand, the basal complexes do not manifest the substantial contraction of the *r*(C–T) bonds to the apex of the pyramid that is observed for the apical structures. The major geometrical changes within the pyramidanes occur within the context of the osme bonds, where the C–T bonds grow longer, in contrast to the contractions that were observed in the apical complexes. Whereas the charge on the T atom had become more negative for apical HBs, somewhat more positive for the XB, and very much more positive for OsB, the pattern is quite different for the basal complexes. The T atom grows more positive for each type of bond, and there are no dramatic differences from one bond type to the next. This increased positive charge is consistent with the idea that density is drawn away from the pyramidane and into the electrophile, as these noncovalent bonds are forged.

The interaction energy decompositions described in Table S8 are also consistent with the idea that all three electrophile types form basically similar noncovalent interactions. The ES percentage is about 50% for Si and Ge, and is reduced a bit for the heavier Sn and Pb. Dispersion contributes another 1/4 or so. POL and CT account for the remainder, with the latter generally being larger than the former.

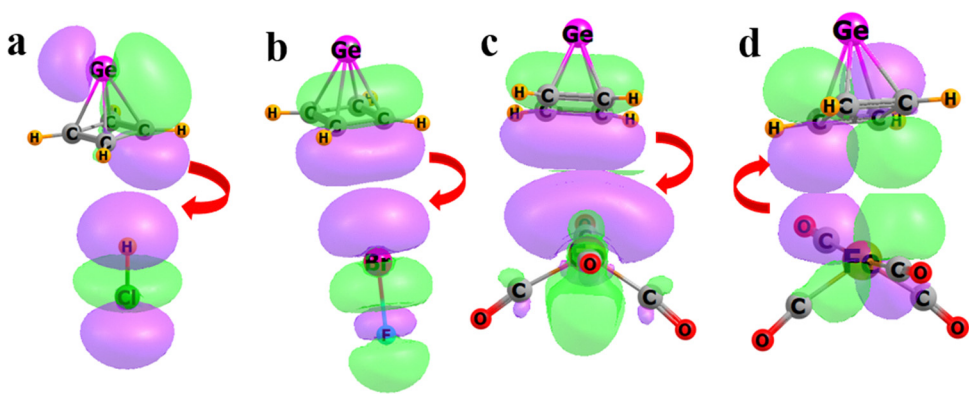

Fig. 7 Natural bond orbitals primarily responsible for the intermolecular bonding of $Ge(CH)_4$ with (a) HCl, (b) BrF, and (c) and (d) $Fe(CO)_4$. Red arrows indicate the direction of electron flow.

Table 8 Interaction energy differences (kcal mol^{-1}) between apical and basal complexes (positive and negative values, respectively, indicate greater and lesser stability of the apical structure)

	$Si(C_4H_4)$		$Ge(C_4H_4)$		$Sn(C_4H_4)$	
	M062X	CCSD(T)	M062X	CCSD(T)	M062X	CCSD(T)
HF	−1.85	−0.80	−2.65	−1.78	−4.31	−3.41
HCl	−2.05	−1.23	−2.54	−1.81	−3.79	−2.78
HBr	−2.04	−1.32	−2.52	−1.79	−3.70	−2.74
FCl	5.63	3.25	−1.17	−0.95	−2.79	−2.35
FBr	7.75	5.85	−0.25	−0.33	−3.48	−3.12
FI	6.39	5.98	0.31	0.38	−2.04	−1.98
$Fe(CO)_4$	17.52	26.20	8.19	14.48	4.62	9.22
$Ru(CO)_4$	20.76	26.06	9.44	14.80	7.16	11.87
$Os(CO)_4$	28.32	30.06	15.09	17.97	12.91	14.91

There will be natural competition between the apical and basal sites for an incoming electrophile. The competitive advantage of the apical over the basal complexes is listed explicitly in Table 8, where the positive values signify the greater stability of the former. It is immediately apparent that the osme bonds greatly prefer the apical T atom, by amounts varying between 4.6 and 28.3 kcal mol^{-1}. One can attribute this advantage to the presence of a strong and partially covalent bond to the T atom. The HBs show a consistent preference for the basal geometries, consonant with the more negative potential minimum at this location within the pyramidanes as compared to the T locale. The pattern is more interesting for the halogen bonds. The Si-pyramidanes favor association with the apical atom, whereas the base is favored over Sn. The situation is mixed for Ge: the lighter Cl and Br prefer the base, whereas I with its deeper σ-hole favors the Ge center. Of course, all three types of electrophiles favor the base of the Pb-pyramidanes as there are no complexes with the apical Pb, with its highly positive MEP.

Discussion

The work detailed here has shown that a tetrel atom positioned at the apex of a square C-pyramid is capable of engaging in a stabilizing interaction with an electrophile. The bonding can be of various types, either hydrogen, halogen, or osme bonding. This bonding occurs through the intermediacy of a pseudo-lone pair that accumulates directly above this apex T. The electrostatic potential at this site is generally negative, as for Si and Ge, but the bonding can occur even in the face of a small positive potential as for Sn. On the other hand, the more positive potential associated with the heavier Pb prevents any of these bonds from forming.

The H-bonds are fairly weak, on the order of 3 kcal mol^{-1} or less, but the halogen bonds are considerably stronger but variable, covering the range between 3 and 14 kcal mol^{-1}. Both the HBs and XBs follow the conventional trends in that the former grow stronger with the acidity of HF, and the latter strengthen as the X atom grows larger and becomes more electropositive. Strongest of all, between 18 and 38 kcal mol^{-1}, and containing a significant degree of covalent character, are the osme bonds to Fe, Ru, and Os. Si engages in the strongest OsBs, with Ge and Sn roughly equivalent. Os forms stronger bonds than does either Fe or Ru. The HBs to Si and Ge are largely dominated by electrostatics, as is a common feature of most such bonds. However, the influence of dispersion grows in importance for Sn. The halogen bonds to the apical T place electrostatics and charge transfer on a roughly equal footing, except for Si where charge transfer plays the dominant role. The osme bonds all contain a heavy dose of electrostatics, regardless of the size of T, and dispersion is nearly negligible.

Because the MEPs of these pyramid shaped molecules are characterized by a negative region at their base, this site attracts the various electrophiles despite the absence of a lone pair in this position. The various electrophiles are drawn instead toward the C–C π-bonding orbitals, which serve as a reservoir of charge that is amenable to transfer. The bonding to the pyramid's base, whether the electrophile is an H, X, or group 8 metal atom, is controlled largely by electrostatics, which accounts for roughly half of the total attraction. Polarization and charge transfer make more minor contributions, even less than dispersion in some cases. Bonding to the group 8 metal atoms is clearly noncovalent and much weaker than when M attacks the T atom at the pyramid apex.

There is an interesting competition between the apex T atom and the all-C base of the pyramid. Perhaps due to their dependence on electrostatics, proton donors are drawn preferentially toward the pyramid base with its more negative potential. These HB energies lie in the 4–6 kcal mol^{-1} range, placing the pyramid base on the same scale as O and N lone pairs as electron donors. HBs to the apex of the pyramid are consistently weaker, some less than even 1 kcal mol^{-1}. On the other end of the spectrum are the osme bonds to the group 8 metals. Their bonding to the pyramid base is substantive but clearly noncovalent, between 5 and 28 kcal mol^{-1}. But their approach toward the apex T leads to much stronger bonding, with a significant covalent contribution. The interaction energies of these coordinate covalent bonds fall in the 18–38 kcal mol^{-1} range. This stronger bonding to the apex occurs despite a disadvantage in terms of a small negative, and even slightly positive, electrostatic potential at the T center. The halogen bonds present the most interesting mix of competitive bond strengths. While the Si apex is favored over the base, this balance shifts toward the base for the heavier Ge and Sn, with their much lower negative potential. Indeed, there are no stable apical complexes at all for Pb with its substantially positive potential.

The results for the various T apex atoms can be compared with prior calculations placing C at this position.[15] The MEP at the C apex was measured to be −42.3 kcal mol^{-1}, considerably larger in magnitude than any of the larger T atoms examined here. Like the systems discussed above, this apical C had associated with it a pseudo-lone pair, which was able to interact with a host of electrophiles. The interaction energies varied up to as high as 57 kcal mol^{-1} for the tetrel bond with SnF_4.

The C···HX HB energies were considerably stronger than those with larger T apices, more than 10 kcal mol^{-1}. The same greater strength was observed for halogen bonds of nearly 30 kcal mol^{-1}. Strongest of all were T···C tetrel bonds to various TF_4 Lewis acids that exceeded 50 kcal mol^{-1}. The bonding of the C-pyramidanes to any of these electrophiles contained a major contribution from electrostatics, in most cases well above 50%. This fraction exceeds that of a number of heavier T-pyramidanes examined here. Veljkovic *et al.* had computed HB energies for C-pyramidanes with water[14] at the CCSD(T)/CBS level. Due to the much more negative potential on the C as opposed to the heavier tetrels here, the energies of these O–H···C HBs were a bit stronger, between −2.0 and −7.4 kcal mol^{-1}. This strength was amplified by the substitution of electron-donating groups on the four basal C atoms.

Lee[9,10] *et al.* had considered other types of pyramidanes where both the apex and base atoms were replaced by tetrels other than C. They identified what they considered to be a high degree of ionicity in the bonds connecting the apex to the base atoms. AIM bond critical point densities for the bonds including the apex are uniformly smaller than those connecting base atoms to one another. This work verified the presence of a very high s-character lone pair on the apex atom. These results were validated in another study,[2] which also provided ELF analyses that mirror our own picture in Fig. 2. Imagawa *et al.*[11] placed Si at the apex and were able to bind this pyramidane with an $Fe(CO)_4$ species and determine the structural data from the crystal. Their observed R(Si···Fe) distance of 2.211 Å was rather close to our calculated bond length of 2.202 Å, confirming the strength of this osme bond. The geometry was also consistent with our computed trigonal bipyramidal structure around the Fe. Other work has considered non-tetrel atoms at the apex of the pyramidane. In various bora[4]pyramidanes,[41] the bond critical point density from B to the base C atoms was larger than 0.1.

Conclusions

The MEPs of T-pyramidanes are characterized by minima at both the apex containing the T atom and the square base of the pyramid. Both of these minima can sustain an interaction with an incoming electrophile, except Pb whose MEP minimum is too positive. The square base forms stronger HBs than does the apex, while it is the latter site containing the T atom that more strongly engages with the group 8 metal atom within $M(CO)_4$. The situation is more nuanced for XBs, which favor T for Si and the square base for Sn; the preference of Ge depends upon the precise nature of M. Regarding the apical interactions with the T pseudo-lone pair, HBs are rather weak, less than 3 kcal mol^{-1}, while XBs are stronger, up to as much as 14 kcal mol^{-1}. Interactions with $M(CO)_4$ are much stronger, ranging up to nearly 40 kcal mol^{-1}, and are partly covalent. Approach of any of the electrophiles to the square base from below presents bonds to the base C–C π-system that are universally noncovalent, not exceeding 17 kcal mol^{-1}.

Author contributions

Conceptualization: M. M. and W. Z.; data curation: M. M. and W. Z.; investigation: S. S., M. M., and W. Z.; visualization: S. S., M. M., and W. Z.; funding acquisition: S. S. and W. Z.; validation: M. M. and W. Z.; writing—original draft: M. M.; writing—review & editing: S. S., M. M., and W. Z.

Conflicts of interest

There are no conflicts to declare.

Data availability

The data supporting this study have been included as part of the supplementary information (SI). Supplementary information includes: NBO diagrams, values of MEP maxima, deformation and binding energies of optimized apical and basal dimers, QTAIM parameters and diagrams for all studied compounds, changes in internal bond lengths and charge on tetrel atom due to complexation, ALMO-EDA results as well as coordinates for optimized structures. See DOI: **https://doi.org/10.1039/d5cp03390j**.

Acknowledgements

The authors gratefully acknowledge the Polish high-performance computing infrastructure PLGrid (HPC Centers: ACK Cyfronet AGH) for providing computer facilities and support through a computational grant (no. PLG/2023/016853), Wrocław Center for Networking and Supercomputing (WCSS). This material is also based upon work supported by the U.S. National Science Foundation under grant no. 1954310 to SS. This work was financed in part by a statutory activity subsidy from the Polish Ministry of Science and Higher Education for the Faculty of Chemistry of Wroclaw University of Science and Technology.

References

1 Q. Sun, C. Muck-Lichtenfeld, G. Kehr and G. Erker, *Nat. Rev. Chem.*, 2023, **7**, 732–746.
2 L. Vidal, D. Barrena-Espes, J. Echeverria, J. Munarriz and A. M. Pendas, *ChemPhysChem*, 2024, **25**, e202400329.
3 V. I. Minkin, R. M. Minyaev, I. I. Zakharov and V. I. Avdeev, *Zh. Org. Khim.*, 1978, **14**, 3–15.
4 V. Y. Lee and O. A. Gapurenko, *Chem. Commun.*, 2023, **59**, 10067–10086.
5 V. I. Minkin, R. M. Minyaev and R. Hoffmann, *Usp. Khim.*, 2002, **71**, 989–1014.
6 E. Lewars, *J. Mol. Struct.*, 1998, **423**, 173–188.
7 J. P. Kenny, K. M. Krueger, J. C. Rienstra-Kiracofe and H. F. Schaefer, *J. Phys. Chem. A*, 2001, **105**, 7745–7750.
8 M. G. Rosenberg and U. H. Brinker, *J. Org. Chem.*, 2021, **86**, 878–891.

9 V. Y. Lee, Y. Ito, A. Sekiguchi, H. Gornitzka, O. A. Gapurenko, V. I. Minkin and R. M. Minyaev, *J. Am. Chem. Soc.*, 2013, **135**, 8794–8797.
10 V. Y. Lee, O. A. Gapurenko, Y. Ito, T. Meguro, H. Sugasawa, A. Sekiguchi, R. M. Minyaev, V. I. Minkin, R. H. Herber and H. Gornitzka, *Organometallics*, 2016, **35**, 346–356.
11 T. Imagawa, L. Giarrana, D. M. Andrada, B. Morgenstern, M. Nakamoto and D. Scheschkewitz, *J. Am. Chem. Soc.*, 2023, **145**, 4757–4764.
12 S. Satpati, T. Roy, S. Giri, A. Anoop, V. S. Thimmakondu and S. Ghosal, *Atoms*, 2023, **11**, 96.
13 V. Y. Lee, J. Wang, T. Sasamori, O. A. Gapurenko, R. M. Minyaev, V. I. Minkin, K. Takeuchi, N. Fukaya and H. Gornitzka, *Chemistry*, 2024, **30**, e202401806.
14 I. S. Veljkovic, M. Malinic and D. Z. Veljkovic, *Phys. Chem. Chem. Phys.*, 2025, **27**, 2563–2569.
15 M. Michalczyk, W. Zierkiewicz and S. Scheiner, *Chem. Sci.*, 2025, **16**, 10572–10584.
16 Q. Sun, C. G. Daniliuc, X. Y. Yu, C. Mück-Lichtenfeld, G. Kehr and G. Erker, *J. Am. Chem. Soc.*, 2022, **144**, 7815–7821.
17 J. S. Murray, P. Lane, T. Clark, K. E. Riley and P. Politzer, *J. Mol. Model.*, 2012, **18**, 541–548.
18 P. Politzer and J. S. Murray, *Crystals*, 2017, **7**, 212.
19 M. Calabrese, A. Pizzi, A. Daolio, R. Beccaria, C. Lo Iacono, S. Scheiner and G. Resnati, *Chem. – Eur. J.*, 2024, **30**, e202304240.
20 R. M. Gomila and A. Frontera, *Inorganics*, 2022, **10**, 133.
21 A. Pizzi, A. Daolio, M. Calabrese, G. Terraneo, A. Frontera and G. Resnati, *Acta Crystallogr., Sect. A: Found. Adv.*, 2021, **77**, C800–C800.
22 X. Wang, Q. Z. Li and S. Scheiner, *Molecules*, 2024, **29**, 79.
23 F. Weigend, *Phys. Chem. Chem. Phys.*, 2006, **8**, 1057–1065.
24 F. Weigend and R. Ahlrichs, *Phys. Chem. Chem. Phys.*, 2005, **7**, 3297–3305.
25 Y. Zhao and D. G. Truhlar, *Acc. Chem. Res.*, 2008, **41**, 157–167.
26 Y. Zhao and D. G. Truhlar, *Theor. Chem. Acc.*, 2008, **120**, 215–241.
27 M. J. Frisch, G. W. Trucks, H. B. Schlegel, G. E. Scuseria, M. A. Robb, J. R. Cheeseman, G. Scalmani, V. Barone, G. A. Petersson, H. Nakatsuji, X. Li, M. Caricato, A. V. Marenich, J. Bloino, B. G. Janesko, R. Gomperts, B. Mennucci, H. P. Hratchian, J. V. Ortiz, A. F. Izmaylov, J. L. Sonnenberg, D. Williams-Young, F. Ding, F. Lipparini, F. Egidi, J. Goings, B. Peng, A. Petrone, T. Henderson, D. Ranasinghe, V. G. Zakrzewski, J. Gao, N. Rega, G. Zheng, W. Liang, M. Hada, M. Ehara, K. Toyota, R. Fukuda, J. Hasegawa, M. Ishida, T. Nakajima, Y. Honda, O. Kitao, H. Nakai, T. Vreven, K. Throssell, J. A. Montgomery Jr., J. E. Peralta, F. Ogliaro, M. J. Bearpark, J. J. Heyd, E. N. Brothers, K. N. Kudin, V. N. Staroverov, T. A. Keith, R. Kobayashi, J. Normand, K. Raghavachari, A. P. Rendell, J. C. Burant, S. S. Iyengar, J. Tomasi, M. Cossi, J. M. Millam, M. Klene, C. Adamo, R. Cammi, J. W. Ochterski, R. L. Martin, K. Morokuma, O. Farkas, J. B. Foresman and D. J. Fox, Wallingford, CT, 2016.
28 S. F. Boys and F. Bernardi, *Mol. Phys.*, 1970, **19**, 553–566.
29 T. Lu and F. Chen, *J. Mol. Graphics Modell.*, 2012, **38**, 314–323.
30 T. Lu and F. Chen, *J. Comput. Chem.*, 2012, **33**, 580–592.
31 B. Silvi and A. Savin, *Nature*, 1994, **371**, 683–686.
32 S. Noury, F. Colonna, A. Savin and B. Silvi, *J. Mol. Struct.*, 1998, **450**, 59–68.
33 W. Humphrey, A. Dalke and K. Schulten, *J. Mol. Graphics*, 1996, **14**, 33–38.
34 R. F. W. Bader, *Atoms in Molecules, A Quantum Theory*, Clarendon Press, Oxford, 1990.
35 R. F. W. Bader, *J. Phys. Chem. A*, 1998, **102**, 7314–7323.
36 T. A. Keith, AIMAll TK Gristmill Software, Overland Park KS, 2013.
37 P. R. Horn, Y. Mao and M. Head-Gordon, *Phys. Chem. Chem. Phys.*, 2016, **18**, 23067–23079.
38 P. R. Horn, Y. Mao and M. Head-Gordon, *J. Chem. Phys.*, 2016, **144**, 114107.
39 F. Weinhold, C. R. Landis and E. D. Glendening, *Int. Rev. Phys. Chem.*, 2016, **35**, 399–440.
40 P. S. V. Kumar, V. Raghavendra and V. Subramanian, *J. Chem. Sci.*, 2016, **128**, 1527–1536.
41 D. J. Luder, N. Terefenko, Q. Sun, H. Eckert, C. Mück-Lichtenfeld, G. Kehr, G. Erker and T. Wiegand, *Chem. – Eur. J.*, 2024, **30**, e202303701.